Physics-Based Compact TDDB Models for Low-*k* BEOL Copper Interconnects With Time-Varying Voltage Stressing

Shaoyi Peng, *Student Member, IEEE*, Han Zhou, *Student Member, IEEE*, Taeyoung Kim, *Member, IEEE*, Hai-Bao Chen, *Member, IEEE*, and Sheldon X.-D. Tan, *Senior Member, IEEE*

***Abstract*— Time-dependent dielectric breakdown (TDDB) is one of the important failure mechanisms for copper (Cu) interconnects. This problem becomes more severe as the pitch between wires is shrinking and low-*k* dielectric materials (low electrical and mechanical strength) are used. Many TDDB models have been proposed based on different physics kinetics in the past. Recently, a physics-based TDDB model, which is based on the breakdown concept of electric path generation, has been proposed and has shown advantage over widely accepted existing electrostatic field-based TDDB assessment. However, determination of the time-to-failure from this model includes time-consuming finite-element method (FEM). In this paper, we try to mitigate this problem by developing fast time to failure evaluation method based on the closed form solution of the ion diffusion partial differential equations. We show that the location of the minimum concentration can be determined by the dominant terms with sufficient accuracy and the time to failure can also be computed with a few dominant terms. On top of this, we also consider the time-varying stressing voltages, which is commonly seen in practical VLSI chips. We propose to develop the equivalent dc stressing voltage, which is parameterized in terms of amplitude, duty cycle, and period for periodic stressing voltage waveforms using regression-based method. We further validate the proposed analytic TDDB concentration and time to failure formula, and the equivalent dc stressing voltage compact model against the results of an FEM analysis using COMSOL. Numerical results further show that the new compact TDDB model can lead to three orders of magnitude speedup with less than 1% error against the existing FEM results.**

***Index Terms*— Dielectric breakdown, integrated circuit interconnections, integrated circuit reliability.**

I. Introduction

With aggressive technology scaling accompanied by employment of new advanced materials, back end of line (BEOL) dielectric reliability, such as time-dependent dielectric breakdown (TDDB) and chip-package interaction (CPI), has become more significant due to the introduction of low-*k*, ultralow-*k*, or even porous dielectrics in advanced technology interconnects, which have poorer thermal and mechanical properties compared to traditional SiO2 dielectrics. According to the 2015 International Technology Roadmap for Semiconductor for Interconnect [1], TDDB is one of the top three interconnect reliability challenges the semiconductor industry faces (the other two are electromigration and stress-induced voiding, which are mainly metal reliability) for Cu/low-*k* interconnect technology. TDDB is the physical phenomenon that a dielectric will break down with time when the dielectric deposited under a field becomes weaker than the material breakdown strength. TDDB has become a serious dielectric reliability concern and failure mechanism for BEOL interconnects, so accurate and fast modeling and estimation of TDDB failure become important.

Traditionally, TDDB is a major concern for the gate oxide of CMOS devices. However, with aggressive technology scaling accompanied by the employment of new advanced low-*k* and even porous materials, TDDB becomes a serious reliability concern and failure mechanism for BEOL interconnects [1], [2]. The dielectric breakdown is caused by the conducting path formation through the intermetal dielectric (IMD) oxide between metal lines from electron tunneling current. Finally, a significant large leakage current occurs and results in the chip operation failure. TDDB effects can be seen at the interlayer dielectric (ILD) between two metal layers and IMD between metal lines in the same layer of the low-*k* dielectrics. In general, due to the fact that ILD space is larger than the space between metal lines, we focus on TDDB in IMD in this paper. Fig. 1(a) shows the structure of two metal lines.

Previously, TDDB had only been a problem with very thin gate oxides and was never an issue in IMD between metals as the thickness of the dielectric was much thicker than the gate and intermetal silicon dioxide of high electric strength is used. However, with the scaling-down of feature size and the introduction of low-*k* and even porous dielectrics with low breakdown strengths for advanced BEOL interconnects, the picture starts to change. For instance, current leading edge CMOS technology development focuses on 10- and 7-nm nodes, where line-to-line/via spacings below 20 nm and dielectrics with a *k*-value below 2.55 (compared to the normal value of 4 for silicon dioxide) are being integrated [4]. Fig. 1(b) shows

Manuscript received April 12, 2017; revised July 6, 2017 and September 3, 2017; accepted October 4, 2017. Date of publication November 14, 2017; date of current version January 19, 2018. This work was supported in part by NSF under Grant CCF-1527324, in part by UC-Mexus under Grant CN 16–161, and in part by the Nature Science Foundation of China under Grant 61604095. *(Corresponding author: Sheldon X.-D. Tan.)*

S. Peng, H. Zhou, and S. X.-D. Tan are with the Department of Electrical and Computer Engineering, University of California at Riverside, Riverside, CA 92521 USA (e-mail: stan@ece.ucr.edu).

T. Kim is with the Department of Computer Science and Engineering, University of California at Riverside, Riverside, CA 92521 USA.

H.-B. Chen is with the Department of Micro/Nano Electronics Engineering, Shanghai Jiao Tong University, Shanghai 200240, China.

Color versions of one or more of the figures in this paper are available online at http://ieeexplore.ieee.org.

Digital Object Identifier 10.1109/TVLSI.2017.2764880

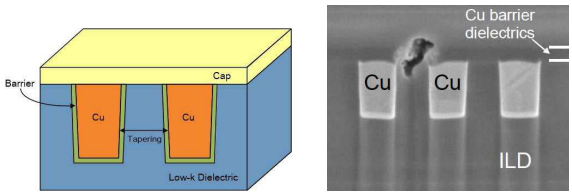

(a) (b)

Fig. 1. Cross section of (a) copper/low-k dielectric structure and (b) SEM image after TDDB failure, courtesy of [3].

the typical scanning electron microscopy (SEM) image after the TDDB failure [3].

TDDB effects have been intensively studied in the past, and many TDDB models have been proposed based on different breakdown mechanisms such as E, $1/E$, and $E^{1/2}$ models. The E-model describes a weak bond breakage due to thermo-chemical heating [5]. The $1/E$-model describes high energy hole injection-induced failure [6]. These models were initially introduced for gate oxides and later examined for the extension to the copper/low-k interconnects. The $E^{1/2}$-model has been first proposed for metal–SiN–metal capacitors [7] and later examined in the low-k TDDB by assuming that the copper ion plays an important role in the dielectric breakdown [3], [8]. Recently, some studies show that the migration of copper ions is not significant due to the existence of copper barrier (i.e., Ta). Instead, the barrier ions play an important role in ion migration [9]–[11]. Moreover, the breakdown depends on the conducting path formation between the two metal lines. However, the majority of currently employed TDDB assessment approaches are based on calculations of the across-layout electrostatic fields and, thus, cannot provide any kind of the interconnect lifetime assessment.

Recently, a TDDB assessment method has been introduced by assuming a constant voltage drop between all neighboring metal segments for their TDDB analysis [12]. For practical VLSI chips, the voltages at some wires are not constant as the powers of a chip are load-dependent. As a result, their TDDB impacts on low-k dielectrics need to be considered. The electric fields between neighboring signal lines are time-dependent waveforms. Thus, the existing proposed method in [12] will result in too conservative analysis. To mitigate this problem, a more accurate physics-based TDDB assessment in back end on-chip interconnects has been proposed recently in [11]. The method is based on the breakdown concept of a complementary combination of electric current path generation by means of diffusing metal ions and field-based hoping conductivity of the current carriers, which was shown to have advantage over widely accepted existing electrostatic field-based TDDB assessment techniques and the model agrees well with measured results in publication [11].

However, this method needs to simulate the electric path generation (EPG) by solving the partial differential equation of ion diffusion process with complicated numerical analysis methods, such as a finite-element method (FEM). For practical VLSI chips, there are many layout patterns or feature with different intermetal spacings, corners, turnings, misaligned vias under different voltages, and temperatures stressing conditions, such an FEM-based numerical analysis method will not be very scalable, if impossible, for full-chip TDDB analysis with a large number of interconnect patterns. Thus, we need to have a much more efficient assessment technique and compact model for fast TDDB analysis. Furthermore, for practical VLSI chips, especially the signal wires, the voltage between them depends on the switching activities and input loads. As a result, we have to consider the time-varying stressing voltage for accurate TDDB assessment. However, most of the proposed existing models do not consider this issue as almost all of them assume constant electric field or voltages. This is also true for the proposed EPG model [11].

In this paper, we try to resolve the mentioned problem by developing a fast TDDB time to failure (TTF) evaluation technique based on the EPG TDDB model. We first show that the exact analytic solutions can be found for the proposed partial differential equations of ion diffusions in the 1-D case with proper boundary conditions. Then, we show that the location of the minimum ion concentration can be further determined analytically by the dominant terms and the time to failure can be computed by using a few dominant terms with sufficient accuracy. Details of a mathematical derivation process for the proposed TDDB compact models will be given. On top of this, we also consider the time-varying stressing voltages, which are commonly seen in practical VLSI chips. We propose to compute an equivalent dc stressing voltage for given time-varying stressing voltages such that both voltages will lead to the same time to failure for the same wire structure. The developed equivalent dc stressing voltage is parameterized in terms of amplitude, duty cycle, and period for periodic stressing voltage waveforms using a regression-based method. We further show that the proposed EPG TDDB model fits well into the power-law model in the context of existing TDDB models, and validate the proposed fast TTF evaluation method and the equivalent dc stressing voltage compact model against the results of FEM analysis from COMSOL. Numerical results further show that the new compact TDDB model can lead to three order of magnitude speedup with less than 1% error against the existing FEM results.

This paper is organized as follows. Section II reviews the EPG TDDB model. A new way to analyze the ion concentration in this model is proposed in Section III, and some methods of evaluating TTF based on ion concentration are proposed. A method to calculate equivalent dc stressing voltage for common time-varying stress is then introduced in Section IV. Experiment results are shown in Section V and this paper is concluded in Section VI. Detailed derivation for the proposed TDDB compact models is shown in the Appendix.

II. Review of Physics-Based TDDB EPG Model for Low-k BEOL Interconnects

In this section, the recently proposed EPG TDDB model is reviewed. In this model, the dielectric breakdown is considered as the complementary combination of electric current path generation by means of diffusing metal ions and field-based hopping conductivity of the current carriers. As a result, it replaces the widely accepted across-layout electrostatic

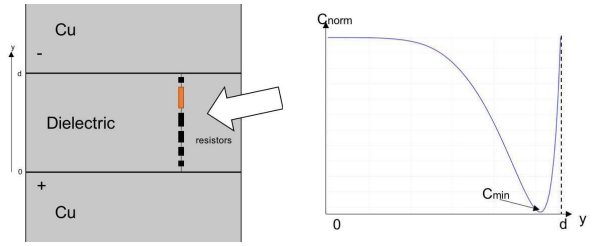

(a) (b)

Fig. 2. (a) Resistors in IMD along $(0, d)$. (b) Distribution of corresponding ion concentration.

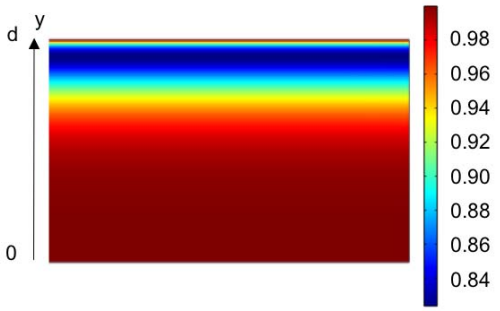

Fig. 3. Distribution of ion concentrations in one pattern.

field-based TDDB assessment. TTF is then determined by the kinetics of the electric current path generation, which is controlled by a time-dependent minimum metal ion concentration in the IMD gap-fill. So in this model, we assume that the barrier metal ions will be injected into the dielectrics based on the recent observation [9].

Specifically, we consider 2-D diffusion of the metal ions along the cap/IMD interface between the oppositely charged metal lines [as shown in Fig. 1(a)], because experiments demonstrate that TDDB failures take place mostly at this interface [13], [14].

In the model, an electric conductivity is represented by electron jumps between neighboring centers (hoping conductivity), which is caused by the injected barrier metal ions like Ta (Tantalum) as mentioned before. As a result, a local conductivity is proportional to the probability of the electron jumping between the neighbor centers, which exponentially depends on the distance between the centers [15]

$$\sigma_{ij} \sim \Gamma_{ij} = \gamma_{ij}^{0} \exp\left\{-\frac{2r_{ij}}{a} - \frac{\varepsilon_{ij}}{k_B T}\right\} \tag{1}$$

where r_{ij} is the distance between i and j centers, a is the radius of electron localization at this type of centers (analog of Bohr's radius), which can reach 100Å, ε_{ij} is the energy barrier between centers, and $k_B T$ is the thermal energy. All connected centers form the resistors network, with the resistor between i and j centers equals to

$$R_{ij} = R_{ij}^{0} \exp\left\{\frac{2r_{ij}}{a} + \frac{\varepsilon_{ij}}{k_B T}\right\}. \tag{2}$$

In a 2-D system, the distance r_{ij} is determined by: $r_{ij} = C(x, y, t)^{-(1/2)}$, where $C(x, y, t)$ is the ion concentration at the considered interface. Fig. 2 shows the schematic of the distribution of ion concentration and corresponding resistor network at an arbitrary instance in time in IMD along a path $(0, d)$ connecting metal electrodes. It is clear that electrons moving from the cathode to anode will meet the biggest resistors at the locations characterized by the largest distances between centers. Since the difference in the distances between centers results in an exponentially large difference in the resistors, it is reasonable to conclude that the total resistance of the path $(0, d)$ depends on the largest resistor, i.e., the minimum ion concentration. Fig. 3 shows the COMSOL FEM analysis result of the distribution of ion concentration for the pattern in Fig. 2(a) under some time of stressing, which is a 2-D version of Fig. 2(b).

The distribution of the normalized ion concentration $C_{\text{norm}}(x, y, t) = C(x, y, t)/C_0$ is governed by the diffusion of ions in an electric field [16]

$$\frac{\partial C_{\text{norm}}}{\partial t} = -\nabla J, \quad \text{where } J = -D\nabla C_{\text{norm}} + \upsilon_d C_{\text{norm}} \tag{3}$$

subject to the following boundary conditions:

$$C_{\text{norm}}(x = 0) = C_{\text{norm}}(x = d) = 1.$$

Here J is the metal flux, $D = D_0 \exp, (-Ea/k_B T)$ is the diffusion coefficient, and $\upsilon_d = E(Dq/k_B T)$ is the metal ion drifting velocity. Ea is the activation energy for metal ion diffusion, k_B is Boltzmann's constant, T is the temperature, q is the electric charge, and E is the electric field.

The developed model of the EPG and evolution allows derivation of the formalism of the leakage current evolution. As mentioned above, the neighboring ions characterized by the largest separation provide the largest "resistivity" for the electrons hopping between metal ions. Assuming that the potential barriers between neighboring centers do not depend on the distance between them ($\varepsilon_{ij} = \varepsilon$), and accepting the Poole–Frenkel mechanism of the field-induced barrier lowering, we can derive the expression for the current density evolution

$$j(t) = j_0 E \exp\left\{-\frac{2}{a\sqrt{C_{\text{norm}}^{\min}(t) \cdot C_0}} - \frac{\varepsilon - q\sqrt{qE/(\pi \varepsilon_{\text{perm}})}}{k_B T}\right\} \tag{4}$$

where $\varepsilon_{\text{perm}}$ is the dielectric dynamic permittivity. The total leakage current can be obtained by integration of leakage current density over the whole shape contour. It was shown in [11] that the EPG model agrees with some observed experimental results in terms of breakdown leakage currents over time, as shown in Fig. 4.

III. New TDDB Analysis Method of EPG Model

A. Derivation of the Analytic Expression for Ion Concentration Distribution in the IMD

In this section, we present a new way to analyze ion concentration and TTF in the EPG model from the solution of the ion diffusion equation (3). Before proceeding, we show that

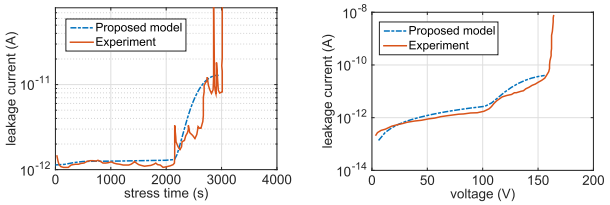

(a) (b)

Fig. 4. Current-voltage leakage changes for (a) constant voltage (TDDB) stress and (b) ramped voltage stress, with experimental data from [17], courtesy of [11].

(a) (b)

Fig. 5. Two example patterns with the same minimum distance (50 nm) studied in the FEM analysis using COMSOL. (a) Straight line. (b) L shape.

TABLE I
PARAMETERS AND CONSTANTS USED

Paras	Value	Paras	Value
D_0	2.24×10^{-11}m^2/s	E_a	0.8eV
$\varepsilon_{\text{perm}}$	2.9	k_B	1.38×10^{-23}J/K
T	370K	V_{DD}	1V

the minimum distance between metal wires is the dominant factor in determining the TTF.

The FEM analysis of (3) using COMSOL has been performed to calculate TTFs of 552 different patterns. In this test, we use $C_x = 0.95$ as the threshold normalized minimum concentration leading to failure. Two example patterns with the same minimum distance between two metals are shown in Fig. 5. In the figure, two gray lines are metal lines, of which one is connected to V_{DD} (supply voltage), and the other is connected to GND (ground), and the white area is the dielectric. The parameters and constants used in the FEM analysis are shown in Table I. The diffusion coefficient D_0 and activation energy E_a are obtained from fitting the experimental results in [17], as shown in Fig. 4.

First, we have tested with patterns with minimum distance of 50 nm. The results are listed in Table II, where *Count* means the number of patterns with the corresponding TTF value. Table II shows the TTFs for most cases are in the range between 360 000 and 41 000 s for the minimum spacing of 50 nm. We want to state that D_0 and E_a have huge impacts on the TTFs of TDDB as they determine the diffusion speeds of the barrier metal ions. We changed the two parameters and the results are shown in Table III.

Table IV shows that the TTF range is between 58 000 and 65 000 s for minimum spacing of 20 nm. The precision of this range is limited by the timestep set in

TABLE II
STATISTICS OF TTFS IN DIFFERENT PATTERNS WITH THE SAME MINIMUM DISTANCE (50 nm)

TTF(s)	Count	Percentage
360000	42	7.61%
370000	269	48.73%
380000	194	35.14%
390000	34	6.16%
400000	11	1.99%
410000	2	0.04%

TABLE III
TTF RESULTS AFTER CHANGING D_0 OR E_a

Test cases	TTF(s)
Original case	363426
D_0 increased by 10%	327083
D_0 decreased by 10%	399767
E_a increased by 10%	6113735
E_a decreased by 10%	21604

TABLE IV
STATISTICS OF TTFS IN DIFFERENT PATTERNS WITH THE SAME MINIMUM DISTANCE (20 nm)

TTF(s)	Count	Percentage
58000	23	4.17%
59000	159	28.80%
60000	219	39.67%
61000	78	14.13%
62000	30	5.43%
63000	12	2.17%
64000	18	3.26%
65000	13	2.36%

COMSOL. As we can see that the layer pattern has some impact on the TTF values, this impact gets bigger for smaller minimum spacing. But for both 50- and 20-nm minimum spacings, the impact on TTF is quite small for the majority of the patterns. We also observed that the minimum spacing dominant effect becomes more obvious when the length of the wires is sufficiently long (compared to the spacing between them). Based on this observation, as the first-order approximation, we can simplify the original problem to the 1-D problem with two parallel metal lines separated by the minimum distance like the one shown in Figs. 2(a) and 5(a), which is the starting point of this paper.

To simplify the notation, we define normalized concentration $C_{\text{norm}}(x,t)$ as $C(x,t)$ for the sake of better presentation. Then, (3) can be rewritten as

$$D\nabla^2 C = \frac{qD}{k_B T}\nabla(C \cdot E) + \frac{\partial C}{\partial t} \tag{5}$$

with boundary condition

$$C(\text{at the edge of dielectric}) = 1 \tag{6}$$

and initial condition

$$C(t = 0, \text{ within the dielectric}) = 0. \tag{7}$$

Equation (5) can be further simplified to 1-D form given the previous discussion as follows:

$$D\frac{\partial^2 C}{\partial x^2} = \frac{qDE}{k_B T}\cdot\frac{\partial C}{\partial x} + \frac{\partial C}{\partial t} \tag{8}$$

with boundary condition

$$C(x=0) = C(x=L) = 1 \tag{9}$$

and initial condition

$$C(x,t) = 0, \quad 0 < x < L, \ t = 0. \tag{10}$$

If we further define X, T', λ, and L

$$X = \frac{x}{L}, \quad T' = \frac{Dt}{L^2}, \quad \lambda = \frac{P_e}{2} = \frac{qE}{2k_B T} \quad L = \frac{qV_{\mathrm{DD}}}{2k_B T}. \tag{11}$$

Equation (8) can be written as

$$\frac{\partial^2 C}{\partial X^2} = P_e\frac{\partial C}{\partial X} + \frac{\partial C}{\partial T'}. \tag{12}$$

The solution of (12) can be found by using Laplace transformation-based method, as shown in the following. The detailed derivation of the solution can be found at the Appendix

$$C(X,T') = 1 - 2\pi\sum_{n=1}^{\infty}\frac{n\sin(n\pi X)}{(n^2\pi^2+\lambda^2)}e^{-(n^2\pi^2+\lambda^2)T'} \cdot [e^{\lambda X} - (-1)^n e^{\lambda X-\lambda}]. \tag{13}$$

We note that (13) is an exact solution without any approximation.

B. TDDB Time to Failure Estimation

In this section, we propose three different methods to estimate TTF based on different approximation of (13). An easy yet inaccurate method is first introduced, followed by an accurate but inefficient version. Finally, we introduce a combined method of these two that is both accurate enough and efficient.

Before proceeding, it is worthwhile to note that the goal here is to find TTF, which is the time when $\min[C(X,\mathrm{TTF})]$ reaches the threshold normalized minimum concentration C_X for $0 < X < 1$.

As (13) contains an infinite series, it is not possible to get an analytical result of TTF. However, numerical methods are still feasible. First, it is natural to consider using first-term approximation because of its simplicity. The first-term approximation of (13) is

$$C_1(X,T') = 1 - \frac{2\pi\sin(\pi X)}{\lambda^2+\pi^2}e^{-(\lambda^2+\pi^2)T'}(e^{\lambda X}+e^{\lambda X-\lambda}). \tag{14}$$

This equation can be used to derive where the minimum concentration locates (let us call it X_{fail}) by calculating the partial derivative of concentration with respect to X and solve for the zero points. Then, we can get a fixed X_{fail}, which does not change with T'. Then, X_{fail} can be used back in (14) to solve for TTF, which gives the result

$$X_{\mathrm{fail}} = 1 - \frac{1}{\pi}\arctan\left(\frac{\pi}{\lambda}\right) \tag{15}$$

$$t_{\mathrm{fail}} = \frac{L^2}{D(\lambda^2+\pi^2)} \times \ln\frac{2\pi^2(e^{\lambda-(\lambda/\pi)\arctan(\pi/\lambda)}+e^{-(\lambda/\pi)\arctan(\pi/\lambda)})}{(1-C_X)(\lambda^2+\pi^2)^{3/2}}. \tag{16}$$

The details of this derivation can be found at the Appendix. This is the first method to evaluate TTF. However, the results from (16) are not accurate, as shown in Section V.

The second method, which is quite accurate, contains two iterative phases, namely, X and T' phases. First, in order to conduct sufficiently accurate approximation of (13), it is preferred to use a large number of terms (here, we use 10 000 terms in our experiments) of the infinite series. Then, because the concentration is monotonically increasing with respect to T', bisection method can be used to numerically derive TTF efficiently in condition that X is fixed. This is the T' phase, which is named because it solves T' with X fixed. Issues about X_{fail} can be tackled by the fact that there exists only one minimum value of concentration with respect to X. Therefore, in X phase, X_{fail} can be searched step by step with a fixed T' from the previous T' phase. In detail, we decrease or increase X with a small enough X_{step} in each searching step until the minimum concentration at X_{fail} is found. Then, a new T' phase may be started for more accurate TTF. A final result can be derived by performing two phases iteratively for only a few times.

This is the most accurate yet most complicated method. In fact, we can combine the previous two methods together to get an accurate and simple method.

As discussed above, bisection method can be used to numerically find TTF if we use three or five terms for approximation. Here, an odd number of terms is used, because the function of concentration has to be monotonic. At the same time, X_{fail} given by (15) can be directly used, so X phase can be skipped. In Section V, we show that results derived from this simple method are quite accurate.

A pseudocode describing this evaluation flowthrough bisection method is listed in Algorithm 1. $C_{\min}(T')$ stands for the ion concentration calculated through a certain approximation of (13) (for example, three-term approximation), with $X = X_{\mathrm{fail}}$ from (15).

C. Study of the Relationship Between TTF and Electric Field

In this section, we study the relationship between the TTF and stressing electric filed or voltage for the proposed TDDB model. We show that the proposed EPG TDDB shows similar relationship between TTF and electric field of the power-law model shown in the following [10], [18]:

$$\mathrm{TTF} = B(T)V^N. \tag{17}$$

To illustrate this, we calculate the TTF with the most accurate method introduced in Section III-B over different electric fields. The pattern studied is still the same pattern we are studying above. We only sweep supply voltage V_{DD} so that electric field can be changed. Fitted coefficients of the power-law model under different temperatures are shown in Table V. Fig. 6 shows the TTF predicted by the fitting power-law models against our EPG models under different temperatures.

Algorithm 1 Evaluation of TTF

```
Set parameters such as spacing L, stressing voltage V_DD
Calculate X_fail from equation (15)
Set initial T' = 1, result error tolerance eps
while C_min(T') < C_X do
    T' = T' * 2
end while
a = 0, b = T', c = (a + b)/2
while b − a < eps do
    if (C_min(a) − C_X) * (C_min(c) − C_X) < 0 then
        b = c, c = (a + b)/2
    else if (C_min(b) − C_X) * (C_min(c) − C_X) < 0 then
        a = c, c = (a + b)/2
    else
        break
    end if
end while
T'_fail = c
```

TABLE V
FITTED COEFFICIENTS OF THE POWER-LAW MODEL

Temperature(K)	$B(T)$	N
370	exp(12.839)	-0.928
390	exp(11.612)	-0.914
410	exp(10.508)	-0.9

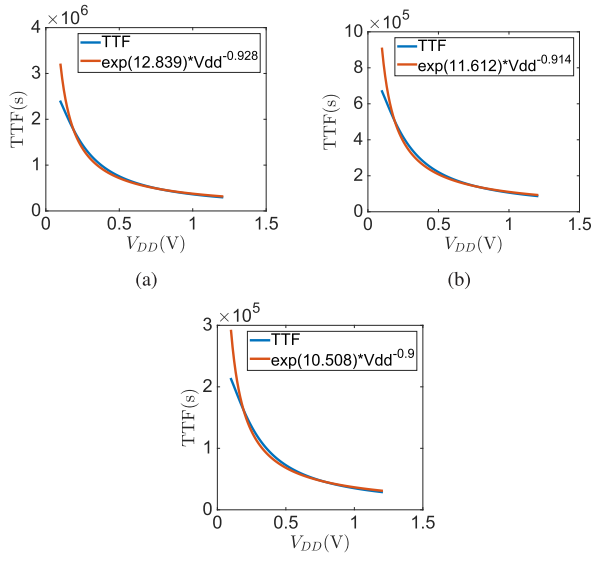

Fig. 6. TTF against different stressing voltages (V_{DD}) in the temperature of (a) 370, (b) 390, and (c) 410 K.

We can see that the calculated voltage exponent N is around 0.9 for different temperatures, which is quite smaller than other power-law models with N ranging from 40 to 48 [10] or even 24–36 [18]. In addition, the recent experimental data from the published BEOL TDDB power-law models show that the exponent N is around 20–24 [19], [20]. We remark that the obtained exponent N and the life times, as shown in Fig. 6, from the fitted power-law models are still far from some observed experimental data. We will continue to further improve the proposed conduction-based TDDB model so that they can be more consistent with the experimental data in the future.

IV. NEW EQUIVALENT DC STRESSING VOLTAGE ANALYSIS OF EPG MODEL

In this section, we present the new equivalent dc stressing voltage model to deal with time-varying stressing voltage in the practical VLSI interconnects.

In the previous discussion, it is assumed that two metal lines in the pattern are connected to V_{DD} and GND, respectively. In real digital ICs, this scenario does not apply to every two neighboring lines, as there are more kinds of metal lines, such as clock net and signal net. However, we can still assume that the voltages on both lines can be described as dc or a square wave. With this being said, it is obvious that the electric field within the IMD can be described as a square wave. For simplicity, we assume it to be unipolar and it can cover the cases, where voltage of one metal line is constant. Three variables can be used to define this unipolar square wave: amplitude, period, and duty cycle. With these three variables, we try to find a function to convert any unipolar square wave to equivalent dc stressing provided that they result in the same TTF. Other cases resulting in bipolar square wave can be treated with the same method, but with one more variable.

Before moving on, we first review the response surface method (RSM), which is used in this paper. The RSM, consisting of a group of mathematical and statistical techniques, explores the relationships between several input variables and one or more responses. Based on a set of designed experiments, an optimal response can be obtained [21]. Specifically in RSM, input parameters are called independent variables and performance measure is considered as a response. Response y depends on input-independent variables $(\xi_1, \xi_2, \ldots, \xi_k)$

$$y = f(\xi_1, \xi_2, \ldots, \xi_k) + \varepsilon \tag{18}$$

where f is the true response function which is unknown and could be very complicated and ε is an error of the model. Usually, a low-order polynomial in some relatively small region of the independent variable space is appropriate. The first-order model and second-order model are the most commonly used models in the RSM. In this paper, the second-order model with relatively good accuracy is employed. A second-order response y depending on variables $(x_1, x_2, \ldots, x_k)$ can be written as

$$y = \beta_0 + \sum_{j=1}^{k} \beta_j x_j + \sum_{j=1}^{k} \sum_{i \le j} \beta_{ij} x_i x_j + \varepsilon. \tag{19}$$

Let $x_{k+1} = x_1 x_1, x_{k+2} = x_1 x_2, \ldots, x_{k(k+3)/2-1} = x_{k-1} x_k, x_{k(k+3)/2} = x_k x_k$ and $\beta_{k+1} = \beta_{11}, \beta_{k+2} = \beta_{12}, \ldots,$ then (19) can be expressed as

$$y = \beta_0 + \sum_{j=1}^{q} \beta_j x_j + \varepsilon \tag{20}$$

which is a linear regression model for coefficients $(\beta_0, \beta_1, \ldots, \beta_q)$, where $q = k(k+3)$. With (20), a least square

TABLE VI
RESULTS OF ION CONCENTRATION DERIVED FROM TWO METHODS

Time(s)	x(nm)	FEM	Results from (13)	Error (%)
1×10^5	35.97	0.01377	0.01363	-1.03%
1×10^5	46.56	0.11680	0.11485	-1.68%
2×10^5	11.67	0.99512	0.99527	0.01%
2×10^5	33.62	0.66238	0.66012	-0.34%
3×10^5	20.49	0.99691	0.99754	0.06%
3×10^5	42.83	0.85763	0.85553	-0.24%

method is employed to estimate the regression coefficients in the multiple linear regression model.

We assume that there are n observed responses $y = (y_1, y_2, \ldots, y_n)$ and for each y_i, there are corresponding parameters $x_i = (x_{i1}, x_{i2}, \ldots x_{iq})$. So (20) can be written in matrix notation as follows:

$$y = X\beta + \varepsilon. \tag{21}$$

To solve β in a least square minimization sense, QR decomposition on X is applied. It is shown that $R\beta = Q^T y$. After solving the linear equations, estimated coefficient vector $\hat{\beta}$ can be calculated. In this paper, the input variables x_i are normalized parameters, which include amplitude, period, and duty cycle.

The TTFs for dc stressing voltage are calculated using methods introduced in Section III-B. A lookup table has been built to quickly find the equivalent dc voltage with the given TTF. TTFs for different square wave stressing voltage are derived using COMSOL.

Because of the limitation of timestep in the FEM analysis, the period of square wave must be very long compared to practical cases.

V. EXPERIMENTAL RESULTS AND DISCUSSION

In this section, we show some numerical results and comparisons for the new TDDB analysis methods. All programs run on a workstation with Xeon E5-2698 CPU and 128-GB memory.

First, we show a comparison between the results of concentration from (13) and those from the COMSOL FEM analysis of (3) in Table VI. The data are based on the pattern shown in Fig. 2(a), in which the distance between two metal lines is 50 nm, and temperature is 370 K. The metal line at $x = 0$ is connected to $V_{\rm DD}$ and the line at $x = 50$ is connected to GND. We can see that the proposed closed form expression gives very accurate results compared to COMSOL simulations.

Then, we show the accuracy and calculation CPU time of different methods for TTF based on the same pattern above. And, we use $C_x = 0.95$ as the threshold normalized minimum concentration leading to failure in our experiment. For the comparison, we consider the result using 10 000 terms and the resulting changes in $X_{\rm fail}$ as the golden results. The comparison results are shown in Table VII. In the last four rows, $X_{\rm fail}$ from (15) is used instead of more accurate $X_{\rm fail}$ for the sake of simplicity. Column Err(%) is the relative error compared to the golden. Tims(s) is the CPU times and column Spdup is the speedup against the FEM method.

TABLE VII
TTF FROM DIFFERENT METHODS, THE CALCULATION TIMES, AND SPEEDUP OVER THE FEM

Method	TTF(s)	Err (%)	Time(s)	Spdup
10000 terms with exact X_{fail}	363426	-	8.702	4.94
FEM	370000	1.81%	43.000	–
10000 terms	363221	-0.06%	3.468	12.40
5 terms	363221	-0.06%	0.013	$3.31E3$
3 terms	366562	0.86%	0.009	$4.78E3$
1 term	412568	13.52%	0.004	$1.08E4$

TABLE VIII
PARAMETERS FOR THREE TESTS

Amplitude(V)	Duty cycle	Period(s)
0.9	0.25∼0.85	100000
0.9	0.45	25000∼175000
0.5∼1.3	0.65	140000

As we can see that if we use five terms, the result is sufficient compared to 10 000 terms as they can give almost the same results. If we use just three terms, the results can be very accurate as well. In terms of CPU time and speedup, as we can see, the speedup can range from 15 to 1.08×10^4. If we chose the three-term result, which gives about 0.86% accuracy, then the speedup can be more than three order of magnitude (4.78×10^3).

We have done the same experiment with the spacing of 20 nm using the three-term method. The result of TTF is 58 650 s. Basically, the solution [see (13)] shows that if only spacing changes, then it holds that TTF $\propto L^{-2}$.

At last, but not least, we compare the RSM fitted results for calculating the equivalent dc stressing voltage against different sets of results from COMSOL. The fitted function to calculate equivalent voltage when $T = 370$ K is

$$\begin{aligned} V_{\rm eq} &= 0.4794 + 0.1606X_1 + 0.4675X_2 + 0.0185X_3 \\ &\quad + 0.0075X_1^2 + 0.1563X_1X_2 + 0.0133X_1X_3 \\ &\quad - 0.0323X^2 - 0.0252X_2X_3 - 0.0031X_3^2 \end{aligned} \tag{22}$$

where

$$X_1 = \frac{\text{Amplitude(V)} - 0.9}{0.3} \quad X_2 = \frac{\text{Duty cycle} - 0.54}{0.46}$$
$$X_3 = \frac{\text{Period(s)}/1000 - 120}{80}.$$

Some tests with parameters given in Table VIII have been done to test the correctness of this function. All these test cases are not used in building the rms function. Each time only one of the three variables is changed so a graph showing the impact of this variable can be drawn. The graphs are shown in Fig. 7. In the graphs, the COMSOL results are derived by searching for equivalent dc voltages based on TTF results from COMSOL. We can see that these graphs prove that rms gives a good result for evaluating equivalent dc voltage.

It is worth mentioning that in the cases with the changeable distance between two metal lines, this result can still be used

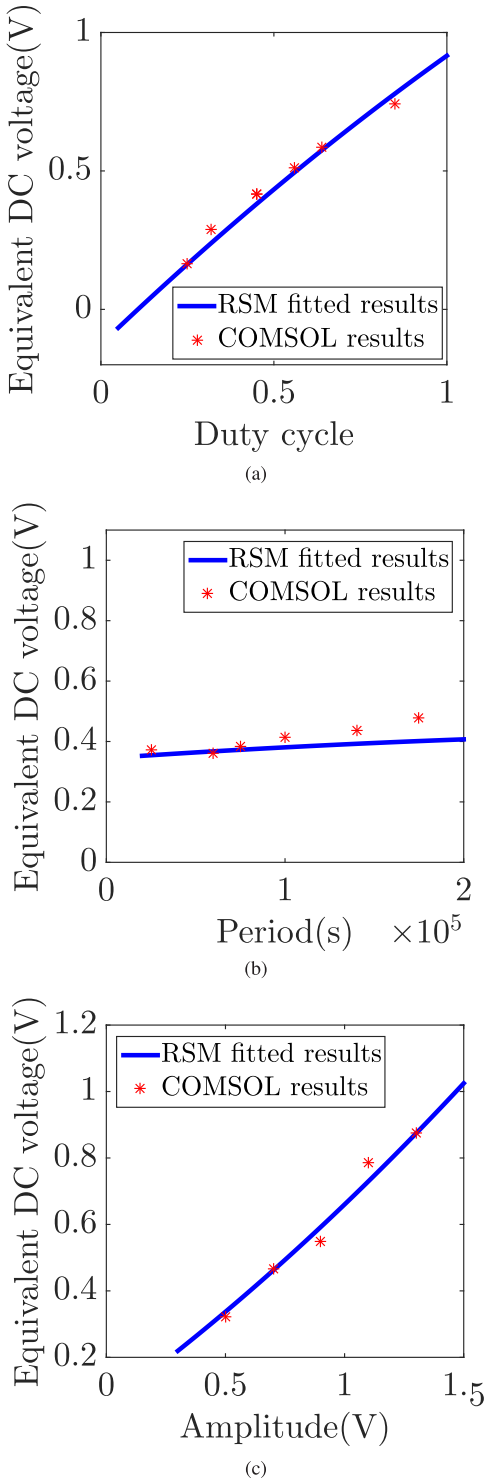

Fig. 7. Comparison between RSM results with COMSOL results on (a) duty cycle, (b) period, and (c) amplitude.

in that the distance L does not appear in (13). The only thing it can affect is the relationship between T' and t, as is introduced in (11). So distance does not change the function of equivalent dc voltage at all.

VI. Conclusion

In this paper, we have proposed a novel compact TDDB model for fast TDDB assessment. We developed a new fast time-to-failure evaluation method based on the analytic solution of the recently proposed ion diffusion partial differential equations. It is showed that the location of the minimum concentration can be determined by the dominant terms and the time-to-failure can be computed by using a few dominant terms. On top of this, we also considered the time-varying stressing voltage, which is commonly seen in practical VLSI chips. We proposed to develop the equivalent dc stressing voltage parameterized by amplitude, duty cycle, and period for periodic stressing voltage waveforms using the regression-based method. We further validated the proposed analytic TDDB concentration and time-to-failure formula and the equivalent dc stressing voltage compact model against the results of the FEM analysis using COMSOL. Numerical results further show the the new compact TDDB model can lead to three orders of magnitude speedup with less than 1% error against the existing FEM results.

Appendix

A. Derivation of the Analytic Solution for the Ion Diffusion Equation

In this section, we give the detailed mathematical derivation of the formulas for the proposed TDDB compact model. For the completeness of this section, we rewrite the metal ion diffusion equation (5) as follows:

$$D\nabla^2 C = \frac{qDE}{k_B T}\nabla C + \frac{\partial C}{\partial t} \tag{23}$$

with the boundary conditions

$$C(\text{at the edge of dielectric}) = 1. \tag{24}$$

In the 1-D case, (23) can be written as

$$D\frac{\partial^2 C}{\partial x^2} = \frac{qDE}{k_B T}\cdot\frac{\partial C}{\partial x} + \frac{\partial C}{\partial t} \tag{25}$$

subject to boundary conditions

$$C(x=0) = C(x=L) = 1 \tag{26}$$

$$C(x,t) = 0, \quad 0 < x < L, \ t = 0. \tag{27}$$

We then define

$$X = \frac{x}{L} \quad T = \frac{Dt}{L^2} \quad P_e = \frac{qE}{k_B T} \quad L = \frac{qV_{\text{dd}}}{k_B T}. \tag{28}$$

Then, we can get

$$\frac{\partial^2 C}{\partial X^2} = P_e\frac{\partial C}{\partial X} + \frac{\partial C}{\partial T'}. \tag{29}$$

After the Laplace transformation, we have

$$\frac{d^2\hat{C}}{dX^2} = P_e\frac{d\hat{C}}{dX} + p\hat{C} \tag{30}$$

subject to boundary conditions

$$\hat{C}(0,p) = \hat{C}(1,p) = \frac{1}{p} \tag{31}$$

where p is the Laplace domain variable. For the differential equation (30), its solution would appear in this following general form:

$$\hat{C} = r_1 e^{p_1 X} + r_2 e^{p_2 X} \tag{32}$$

where p_1 and p_2 are the roots for equation $x^2 = P_e x + p$. As a result, we have $p_{1,2} = (P_e/2) \pm a$ and $a = (P_e^2/4 + p)^{1/2}$ with the following boundary conditions:

$$\begin{cases} r_1 + r_2 = \dfrac{1}{p} \\ r_1 e^{a+P_e/2} + r_2 e^{-a+P_e/2} = \dfrac{1}{p}. \end{cases} \tag{33}$$

By solving for r_1 and r_2, one can obtain the solution in Laplace domain as

$$\hat{C}(p) = \frac{e^{P_e X/2} \sinh[a(1-X)]}{p \sinh(a)} + \frac{e^{P_e(X-1)/2} \sinh(aX)}{p \sinh(a)}. \tag{34}$$

Inverse Laplace transform on (34) is then done to obtain the solution in the time domain. First take a look at the first part of (34), we have

$$\hat{C_1} = \frac{e^{P_e X/2} \sinh[a(1-X)]}{p \sinh(a)}.$$

A property of Laplace transform as this is used here

$$\mathcal{L}^{-1}\{\hat{C}(X, p+b)\} = e^{-bT'} \mathcal{L}^{-1}\{\hat{C}(X, p)\}.$$

Then, we have

$$C_1 = e^{\lambda X - bT'} \cdot \mathcal{L}^{-1} \left\{ \frac{\sinh[p^{1/2}(1-X)]}{(p-b)\sinh(p^{1/2})} \right\} \tag{35}$$

where $b = (P_e^2/4)$, and we assume $\lambda = b^{1/2} = (P_e/2)$. The inverse transform can be derived by adding residues at all poles, in this case there is a pole at $p = b$, and poles at $p^{1/2} = n\pi i, n = 0, \pm 1, \pm 2 \ldots$, or equally $p = -n^2\pi^2$, $n = 0, 1, 2 \ldots$

$$\begin{aligned} &\mathcal{L}^{-1} \left\{ \frac{\sinh[p^{1/2}(1-X)]}{(p-b)\sinh(p^{1/2})} \right\} \\ &= \int_C \frac{\sinh[p^{1/2}(1-X)]}{(p-b)\sinh(p^{1/2})} e^{pT'} dp = \frac{\sinh[\lambda(1-X)]}{\sinh(\lambda)} e^{\lambda^2 T'} \\ &\quad - 2\pi \sum_{n=1}^{\infty} \frac{n \sin(n\pi X)}{(n^2\pi^2 + \lambda^2)} e^{-n^2\pi^2 T'}. \end{aligned} \tag{36}$$

The second part can be treated in the same way. After the inverse transformation, we add two parts and perform some algebraic operations and obtain the final result

$$\begin{aligned} &C(X, T') \\ &= e^{\lambda X} \left\{ \frac{\sinh[\lambda(1-X)]}{\sinh(\lambda)} \right. \\ &\qquad \left. - 2\pi \sum_{n=1}^{\infty} \frac{n \sin(n\pi X)}{(n^2\pi^2 + \lambda^2)} e^{-(n^2\pi^2+\lambda^2)T'} \right\} \\ &\quad + e^{\lambda X - \lambda} \left\{ \frac{\sinh(\lambda X)}{\sinh(\lambda)} + 2\pi \right. \\ &\qquad \left. \times \sum_{n=1}^{\infty} \frac{(-1)^n n \sin(n\pi X)}{(n^2\pi^2 + \lambda^2)} e^{-(n^2\pi^2+\lambda^2)T'} \right\} \\ &= \frac{e^{\lambda X} \sinh[\lambda(1-X)] + e^{\lambda X - \lambda} \sinh(\lambda X)}{\sinh(\lambda)} \\ &\quad - e^{\lambda X} 2\pi \sum_{n=1}^{\infty} \frac{n \sin(n\pi X)}{(n^2\pi^2 + \lambda^2)} e^{-(n^2\pi^2+\lambda^2)T'} \\ &\quad + e^{\lambda X - \lambda} 2\pi \sum_{n=1}^{\infty} \frac{(-1)^n n \sin(n\pi X)}{(n^2\pi^2 + \lambda^2)} e^{-(n^2\pi^2+\lambda^2)T'} \\ &= 1 - 2\pi \sum_{n=1}^{\infty} \frac{n \sin(n\pi X)}{(n^2\pi^2+\lambda^2)} e^{-(n^2\pi^2+\lambda^2)T'} [e^{\lambda X} - (-1)^n e^{\lambda X - \lambda}]. \end{aligned} \tag{37}$$

B. Derivation of Analytic Form for Time to Failure

As approximation, let us take the first term of the analytic solution $C(X, T')$ as $C_1(X, T')$

$$C_1(X, T') = 1 - \frac{2\pi \sin(\pi X)}{\lambda^2 + \pi^2} e^{-(\lambda^2+\pi^2)T'} (e^{\lambda X} + e^{\lambda X - \lambda}). \tag{38}$$

To get the minimum concentration, we set the derivative of $C_1(X, T')$ to zero

$$\begin{aligned} \frac{\partial C_1(X, T')}{\partial X} &= 0 \\ &= \frac{2\pi e^{-(\lambda^2+\pi^2)T'}}{\lambda^2 + \pi^2} e^{\lambda X} (1 + e^{-\lambda}) \\ &\quad \times [\lambda \sin(\pi X) + \pi \cos(\pi X)]. \end{aligned} \tag{39}$$

The solution of this equation gives a fixed X_{fail} which does not change with T' as

$$X_{\text{fail}} = 1 - \frac{1}{\pi} \arctan\left(\frac{\pi}{\lambda}\right). \tag{40}$$

Then at X_{fail}, we define $C(X_{\text{fail}}, T') = C_{\text{fail}}$ as the minimum concentration that triggers the dielectric failure

$$\begin{aligned} C_{\text{fail}} &= 1 - \frac{2\pi e^{-(\lambda^2+\pi^2)T'}}{\lambda^2 + \pi^2} \sin[\pi - \arctan(\pi/\lambda)] \\ &\quad \cdot (e^{\lambda - (\lambda/\pi)\arctan(\pi/\lambda)} + e^{-(\lambda/\pi)\arctan(\pi/\lambda)}) \end{aligned} \tag{41}$$

$$\begin{aligned} &= 1 - \frac{2\pi^2 e^{-(\lambda^2+\pi^2)T'}}{(\lambda^2 + \pi^2)^{3/2}} \\ &\quad \cdot (e^{\lambda - (\lambda/\pi)\arctan(\pi/\lambda)} + e^{-(\lambda/\pi)\arctan(\pi/\lambda)}). \end{aligned} \tag{42}$$

The resulting time to failure can be found by solving

$$\begin{aligned} C_{\text{fail}} &= C_X \\ T'_{\text{fail}} &= \frac{1}{\lambda^2 + \pi^2} \\ &\quad \times \ln \frac{2\pi^2 (e^{\lambda - (\lambda/\pi)\arctan(\pi/\lambda)} + e^{-(\lambda/\pi)\arctan(\pi/\lambda)})}{(1 - C_X)(\lambda^2 + \pi^2)^{3/2}} \\ t_{\text{fail}} &= \frac{L^2}{D(\lambda^2 + \pi^2)} \\ &\quad \times \ln \frac{2\pi^2 (e^{\lambda - (\lambda/\pi)\arctan(\pi/\lambda)} + e^{-(\lambda/\pi)\arctan(\pi/\lambda)})}{(1 - C_X)(\lambda^2 + \pi^2)^{3/2}}. \end{aligned} \tag{43, 44}$$

REFERENCES

[1] *International Technology Roadmap for Semiconductors (ITRS) Interconnect, 2015 Edition*. [Online]. Available: http://www.itrs2.net/itrs-reports.html

[2] S. P. Murarka, M. Eizenberg, and A. K. Sinha, *Interlayer Dielectrics for Semiconductor Technologies*. Boston, MA, USA: Elsevier, 2003.

[3] N. Suzumura *et al.*, "A new TDDB degradation model based on Cu ion drift in Cu interconnect dielectrics," in *Proc. IEEE Int. Rel. Phys. Symp.*, Mar. 2006, pp. 484–489.

[4] K. Croes *et al.*, "Current understanding of BEOL TDDB lifetime models," *ECS J. Solid State Sci. Technol.*, vol. 4, no. 1, pp. N3094–N3097, 2015.

[5] J. W. McPherson and H. C. Mogul, "Underlying physics of the thermochemical *E* model in describing low-field time-dependent dielectric breakdown in SiO_2 thin films," *J. Appl. Phys.*, vol. 84, no. 3, pp. 1513–1523, 1998.

[6] I. C. Chen, S. Holland, and C. Hu, "A quantitative physical model for time-dependent breakdown in SiO_2," in *Proc. IEEE Int. Rel. Phys. Symp.*, Mar. 1985, pp. 26–28.

[7] K.-H. Allers, "Prediction of dielectric reliability from I–V characteristics: Poole–Frenkel conduction mechanism leading to $\sqrt{E}$ model for silicon nitride MIM capacitor," *Microelectron. Rel.*, vol. 44, no. 3, pp. 411–423, 2003.

[8] F. Chen *et al.*, "A comprehensive study of low-*k* SiCOH TDDB phenomena and its reliability lifetime model development," in *Proc. 44th Annu., IEEE Int. Rel. Phys. Symp.*, Mar. 2006, pp. 46–53.

[9] J. C. K. Lam *et al.*, "Evidence of ultra-low-*k* dielectric material degradation and nanostructure alteration of the Cu/ultra-low-*k* interconnects in time-dependent dielectric breakdown failure," *Appl. Phys. Lett.*, vol. 102, no. 2, p. 022908, 2013.

[10] J. W. McPherson, "Time dependent dielectric breakdown physics—Models revisited," *Microelectron. Rel.*, vol. 52, nos. 9–10, pp. 1753–1760, 2012.

[11] X. Huang, V. Sukharev, Z. Qi, T. Kim, and S. X.-D. Tan, "Physics-based full-chip TDDB assessment for BEOL interconnects," in *Proc. Design Autom. Conf.*, Jun. 2016, pp. 1–6.

[12] M. Bashir, D. H. Kim, K. Athikulwongse, S. K. Lim, and L. Milor, "Backend low-*k* TDDB chip reliability simulator," in *Proc. IEEE Int. Rel. Phys. Symp.*, Apr. 2011, pp. 2C.2.1–2C.2.10.

[13] K. B. Yeap *et al.*, "*In situ* study on low-*k* interconnect time-dependent-dielectric-breakdown mechanisms," *J. Appl. Phys.*, vol. 115, no. 12, p. 124101, 2014.

[14] M. Gall, K. B. Yeap, and E. Zschech, "Advanced concepts for TDDB reliability in conjunction with 3D stress," in *Proc. AIP Conf.*, 2014, pp. 79–88.

[15] B. I. Shklovskii and A. L. Efros, *Electronic Properties of Doped Semiconductors*. Berlin, Germany: Springer-Verlag, 1984.

[16] A. S. Grove, *Physics and Technology of Semiconductor Devices*. Hoboken, NJ, USA: Wiley, 1967.

[17] T. L. Tan, C. L. Gan, A. Y. Du, and C. K. Cheng, "Effect of Ta migration from sidewall barrier on leakage current in Cu/SiOCH low-*k* dielectrics," *J. Appl. Phys.*, vol. 106, no. 4, p. 043517, 2009.

[18] E. Y. Wu and J. Sune, "On voltage acceleration models of time to breakdown—Part II: Experimental results and voltage dependence of Weibull slope in the FN regime," *IEEE Trans. Electron Devices*, vol. 56, no. 7, pp. 1442–1450, Jul. 2009.

[19] K. Croes *et al.*, "Low field TDDB of BEOL interconnects using >40 months of data," in *Proc. IEEE Int. Rel. Phys. Symp.*, Apr. 2013, pp. 2F.4.1–2F.4.8.

[20] R. Muralidhar *et al.*, "A stochastic model for impact of LER on BEOL TDDB," in *Proc. IEEE Int. Rel. Phys. Symp.*, Apr. 2017, pp. DG-4.1–DG-4.4.

[21] R. H. Myers and D. C. Montgomery, *Response Surface Methodology: Process and Product Optimization Using Designed Experiments*. Hoboken, NJ, USA: Wiley, 2002.

Shaoyi Peng (S'17) received the B.S. degree in microelectronics from Fudan University, Shanghai, China, in 2016. He is currently working toward the Ph.D. degree at the Department of Electrical and Computer Engineering, University of California at Riverside, Riverside, CA, USA, with a focus on VLSI reliability effect modeling and simulation.

Han Zhou (S'15) received the B.Eng. degree in electronic science and technology from Beijing Jiaotong University, Beijing, China, in 2013 and the M.S. degree in electronic science and technology from the Beijing Institute of Technology, Beijing, China, in 2016. She is currently working toward the Ph.D. degree at the Department of Electrical and Computer Engineering, University of California at Riverside, Riverside, CA, USA, with a focus on VLSI reliability effect modeling, simulation, and optimization.

Taeyoung Kim (S'10–M'17) received the B.S. degree in electronics engineering from Konkuk University, Seoul, South Korea, in 2005, the M.S. degree in electrical engineering from the University of Virginia, Charlottesville, VA, USA, in 2012, and the Ph.D. degree in computer science from the University of California at Riverside, Riverside, CA, USA, in 2017.

He is currently a Software Engineer at Intel Corporation, Hillsboro, OR, USA, where he is involved in signal integrity and power integrity. He has authored or coauthored over 30 papers in scientific journals and conference proceedings. His current research interests include modeling, simulation, and optimization for VLSI circuit reliability, signal integrity, and power integrity.

Dr. Kim received one Best Poster Research Award at the ACM Ph.D. Forum at the Design Automation Conference in 2015. He is an Associate Editor for the *Integration, the VLSI Journal*.

Hai-Bao Chen (M'16) received the B.S. degree in information and computing sciences and the M.S. and Ph.D. degrees in applied mathematics from Xian Jiaotong University, Xian, China, in 2006, 2008, and 2012, respectively.

He then joined Huawei Technologies, Shenzhen, China, where he focused on cloud computing and big data. He was a Postdoctoral Research Fellow at the Electrical Engineering Department, University of California at Riverside, Riverside, CA, USA, from 2013 to 2014. He is currently an Assistant Professor at the Department of Micro/Nano Electronics, Shanghai Jiao Tong University, Shanghai, China. His current research interests include model order reduction, system and control theory, circuit simulation, cloud computing and big data, and electromigration reliability. He has authored or coauthored over 30 papers in scientific journals and conference proceedings.

Dr. Chen received one Best Paper Award Nomination at the Asia and South Pacific Design Automation Conference in 2015. He currently serves as an Associate Editor for the *Integration, the VLSI Journal*.

Sheldon X.-D. Tan (S'96–M'99–SM'06) received the B.S. and M.S. degrees in electrical engineering from Fudan University, Shanghai, China, in 1992 and 1995, respectively, and the Ph.D. degree in electrical and computer engineering from The University of Iowa, Iowa City, A, USA, in 1999.

He is currently a Professor at the Department of Electrical Engineering, University of California at Riverside (UCR), Riverside, CA, USA. He is also a Co-Operative Faculty Member at the Department of Computer Science and Engineering, UCR. He is the Associate Director of the Computer Engineering Program, UCR. His research interests include VLSI reliability modeling, optimization and management at circuit and system levels, thermal modeling, optimization and dynamic thermal management for many-core processors, statistical modeling, simulation and optimization of mixed-signal/RF/analog circuits, parallel circuit simulation techniques based on GPU, and multicore systems.

Dr. Tan received the Outstanding Oversea Investigator Award from the National Natural Science Foundation of China in 2008, the NSF CAREER Award in 2004, the Best Paper Award at the 2007 IEEE International Conference on Computer Design, the Best Paper Award at the 1999 IEEE/ACM Design Automation Conference, three best paper award nominations at the IEEE/ACM Design Automation Conferences in 2005, 2009, and 2014, and one Best Paper Award Nomination at ASP-DAC in 2015. He is currently serving as the Editor-In-Chief for *Integration, The VLSI Journal*. He is also serving as an Associate Editor for two journals: the IEEE TRANSACTION ON VERY LARGE SCALE INTEGRATION SYSTEMS and the *ACM Transaction on Design Automation of Electronic Systems*.